

On-line Supplemental Section

Figure 1 summarizes the injury process of ischemic stroke.

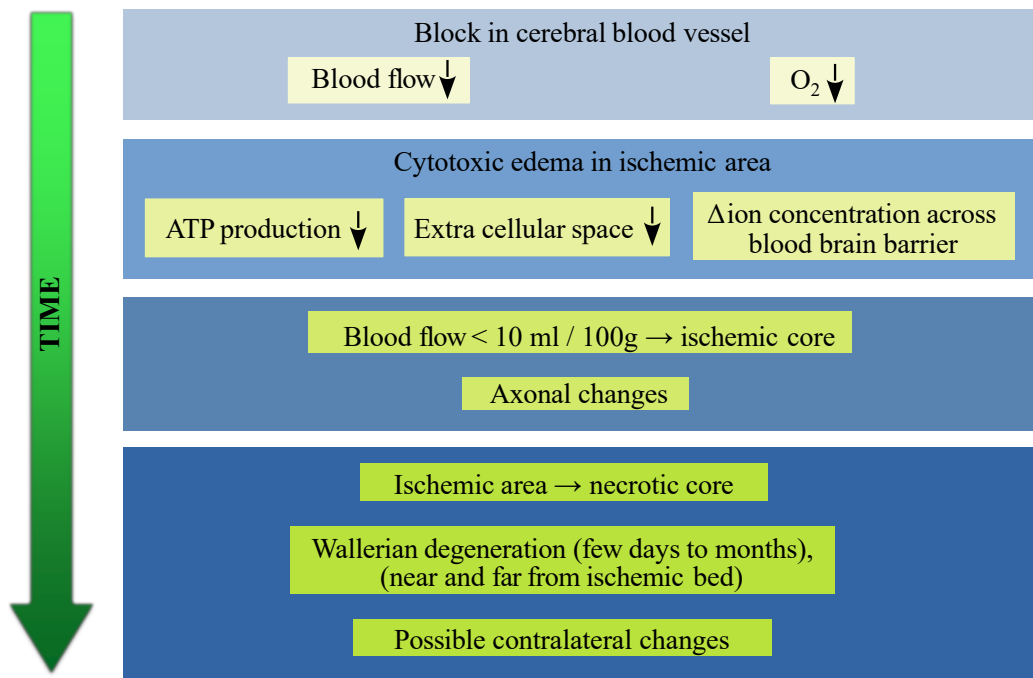


Figure 1: Approximate time course of ischemic stroke.

Figure 2(a) shows an example of a standard trace image and 13 parameter maps from a stroke subject - a 65 year old female imaged 1 week post-stroke with DSI⁹⁶, Fugl-Meyer upper extremity score=29. In Fig. 2(b), the histograms (normalized by number of voxels) are from manually drawn regions on the stroke and mirrored to the contralateral side and are shown to potentially better differentiate the distributions in the stroke and the matching contralateral regions, compared to the differences of the means in the regions.

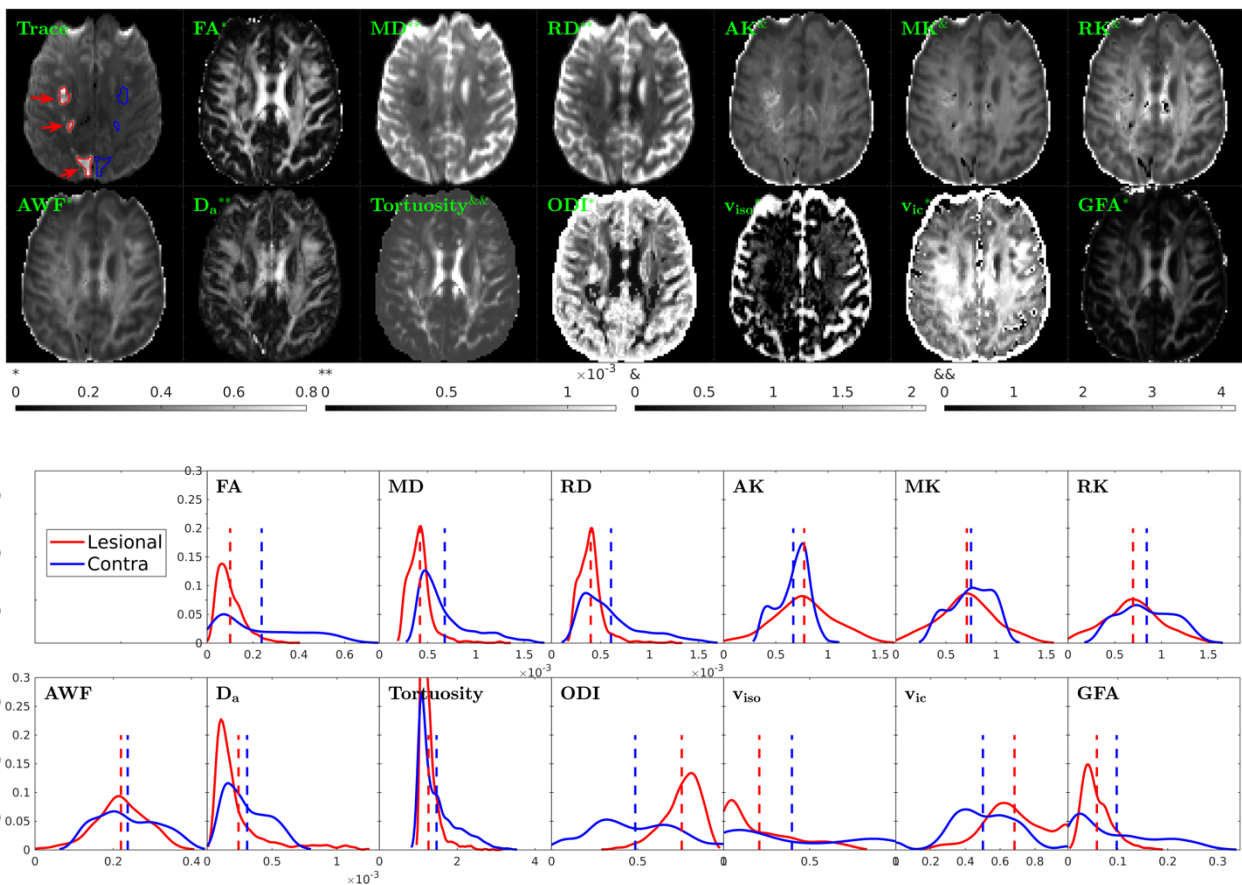


Figure 2: (a) Example of trace (upper left) and 13 parameter maps (see in glossary under DTI, DKI, WMTI, NODDI, and GFA). Stroke regions are marked shown with arrows on the diffusion trace image. The superscripts indicate which grayscale is used with each parameter. These encompass most but not all of the beyond DTI parameters reported in Tables 1-2. (b) Normalized histograms of the parameter distributions in 3D regions drawn in the stroke areas (red) and mirrored on the contralateral side (blue). Dashed lines show the mean values of the regions.

Table 1: Studies using DKI in Stroke Subjects

Paper	Number of subjects	Acquisition directions/b-values	TR/TE (msec)
	Time Points post-stroke		Number of slices
	Scanner		Spatial resolution
	Analysis methods	Outcome measure	Results
Jensen et al. 2011 ¹⁰⁶	3	30/500, 30/1000, 30/1500, 30/2000, 30/2500	1500/104
	13-26 hours		9 slices
	Avanto 1.5T	2x2x5 mm ³	-
	ROIs, DTI, DKI	Percent change from contralesional	Greater changes in MK than MD. Large increases in AK, small in RK
Hui et al. 2012 ⁵	44	30/1000, 30/2000	5500/99
	6 hours to 2 weeks		40 slices
	Avanto 1.5T	3x3x3 mm ³	7 min
	Manual ROIs, DTI, DKI, and WMTI	Percent change from contralesional	MK showed more change than FA. WMTI (in FA>0.3) D _a changed the most
Zhang et al. 2017 ¹⁰⁷	77	25/1250, 25/2500	5000/98
	6 hours to 4 weeks, grouped into 4 intervals		-
	Discovery MR750 3T	1.875x1.875x4 mm ³	5 min 45 sec
	Manual ROIs, DKE	Changes in time post-stroke (unpaired groups)	AK and AD detected changes the best, PLIC most useful region
Chou et al. 2017 ¹⁰⁸	4	8/0, 30/1000, 30/2000, 30/3000	6500/99
	3.3+-0.5 days		25 slices
	GE 1.5T	3x3x3 mm ³	15 min
	ROIs, DKE	Used full 3 shell acquisition as reference	Using only subset of shells gave significant differences

Spampinato et al. 2017 ⁸²	17	10/0, 30/1000, 30/2000	5500/99
	1-4 days		40 slices
	Unspecified 1.5T	3x3x3 mm ³	7 min
	DKE, Fiber tracking to generate ROI of CST	FM at acute and 3 months	Rank correlation=.85 for MK, .78 for AK
Chen et al. 2018 ¹⁰⁹	21 with brainstem stroke	15/1000, 15/2000	6144/109
	Within 72 hours		48 slices
	Ingenia 3T	3mm slice thickness, unreported in-plane	9 min 54 sec
	ROIs at 4 locations. FA, MD, MK	change from contralesional, controls	MK, MD, FA all significantly different from contralesional
Yin et al. 2018 ¹¹⁰	37	20/1000, 20/2000	3300/95
	Two time points: 24 hours, 1 month		20 slices, SMS=2
	Trio 3T	1.6x1.6x5 mm ³ (1.25 mm gap)	2 min 10 sec
	Manual ROIs. FSL, DKE	T2-weighted lesion volumes at 1 month	MK lesion volume at 24 hours closest to outcome measure
Li et al. 2019 ⁸³	43	15/1000, 15/2000	4700/100
	10.1+-2 days		18 slices
	Discovery MR750, 3T	1.875x1.875x3 mm ³ (1.5mm gap)	4 min 12 sec
	Manual ROIs, GE functool	FM, Barthel index	rAK higher in those with ΔFM above recovery threshold
Zhu et al. 2019 ¹¹¹	156	15/1000, 15/2000 NEX=2	6000/162
	Not reported		
	Signa HDe 1.5T	2.5x1.9x5mm3, 1.5mm gap	6 min 18 sec
	Manual ROIs, GE functool	Percent change from contralesional	MK (and AK and RK) larger changes than ADC and FA

Yu et al. 2020 ⁸⁴	48	30/1000, 30/2000	5000/95
	3-7 days		Unreported, ~35 slices
	Discovery MR750, 3T	.94x.94x4 mm ³	Unreported, likely ~6min
	CST tract, voxelwise and slice-wise DKI	Percent change from contralesional. NIHSS motor portion at 3 months	Only AK correlated with NIHSS, r=0.3. FA or MD did not correlate.

Table 1: Studies using DKI in stroke subjects. A total of ten papers with n=450 total subjects. The number of b=0 scans is not included unless the number was clear from the manuscript. For acronyms see Glossary.

Table 2: Studies using GFA, SHORE, rate of kurtosis, or NODDI in stroke subjects

Paper	Number of subjects	Acquisition directions/b-values	TR/TE (msec)
	Time Points post-stroke		Number of slices
	Scanner		Spatial resolution
	Analysis methods	Outcome measure	Results
Tang et al. 2010 ⁸⁸	7	203, max b=6000 (DSI)	9100/142
	90 days		45 slices
	Trio 3T	2.9x2.9x2.9 mm ³	Unreported, likely ~34min
	GFA. ROI or Tract-specific analysis	Lower extremity FM	GFA (only ipsilesional studied) correlates with FM, r~0.8 with ROI or tract-based
Granziera et al. 2012 ⁶	12	258, max b=8000 (DSI)	6600/138
	~1 week, again at 1 month, 6 months		34 slices
	Trio 3T	2.2x2.2x3 mm ³	26 min
	GFA between pairs of motor areas (regions mapped from MPRAGE)	NIHSS motor	Only contralesional studied. GFA+NIHSS+age predictive of 6 month NIHSS, adjusted r ² =.84
Lin et al. 2015 ¹¹²	10, same dataset as Granziera 2012	258, max b=8000 (DSI)	6600/138
	2 timepoints: 1 month, 6 months		34 slices
	Trio 3T	2.2x2.2x3 mm ³	26 min
	GFA between pairs of motor areas (regions mapped from MPRAGE)	NIHSS motor	Only contralesional studied. GFA distribution features depend on NIHSS, age, mRS
Brusini et al. 2016 ⁹¹	10, same dataset as Granziera 2012	258, max b=8000 (DSI)	6600/138
	~1 week, again at 1 month, 6 months		34 slices
	Trio 3T	2.2x2.2x3 mm ³	26 min

	6 SHORE indices	NIHSS motor	Only contralesional studied. All high correlation except RTAP, RTOP best (adjusted $r^2=.98$)
Galazzo et al. 2018 ²⁵	10, same dataset as Granziera 2012	258, max b=8000 (DSI)	6600/138
	~1 week, again at 1 month, 6 months		34 slices
	Trio 3T	2.2x2.2x3 mm ³	26 min
	SHORE indices as in Brusini et al. Also DTI (MD,FA)	NIHSS motor	MD and FA also predict NIHSS well. Most SHORE and DTI also changed in gray matter
Hodgson et al. 2019 ⁹⁶	9	203, max b=4000 (DSI)	3700/114
	3-12 days		51 slices
	Verio 3T	1.9x1.9x2.1 mm ³	13 min (SMS)
	NODDI, GFA, DTI in PLIC, stroke ROI and lesion load	FM at baseline and 38+-9 days post-stroke	ODI in the PLIC the best correlation with FM (optimism adjusted $r^2=0.83$)
Wang et al. 2019 ⁹⁷	71	25/1250, 25/2500	5000/98
	Single time point, groups of: 0-6 hours n=6, 6h-3days n=23, 3days-2 weeks, n=42		
	Discovery MR750 3T	1.875x1.875x4 mm ³	5 min 45 sec
	Stroke ROIs, DKE, DTI, DKI, NODDI	Unpaired changes in parameters at different times post-stroke	ODI changes the most over hours to 2 weeks times post-stroke (unpaired) – and ODI more sensitive than DTI or DKI

Mastropietro et al. 2019⁷	17	12/0, 20/700, 64/2000	16,900 ms/96 ms
	~2 weeks, 10 rescanned at ~8 months		64 slices
	Verio 3T	2x2x2 mm ³	96x16.9=27min
	DTI, DKI, NODDI in PLIC and CP	Change from contralesional	FA, AD, RD, KA, AK, and ODI significantly different in ipsi and contra.
Lampinen et al. 2021³⁵	5	12/0, 6/200, 6/500, 6/1000...6/4000, two diffusion times each	2000/105
	~2 days, rescanned at ~9 days and ~100 days		5 slices
	Achieva 3T	2x2x4 mm ³	12 min
	Rate of kurtosis k and MK, ADC and FA in manual ROIs	-	Diffusion time dependence k may predict chronic ADC.

Table 2: Studies using GFA, SHORE, rate of kurtosis, or NODDI in stroke subjects. A total of nine papers, with n=121 total stroke subjects. Note that four papers use the same ~10 subject dataset. Two of the studies also include DKI but are shown only in this table to reduce redundancy. The number of b=0 scans is not included unless the number was clear from the manuscript. For acronyms see Glossary.

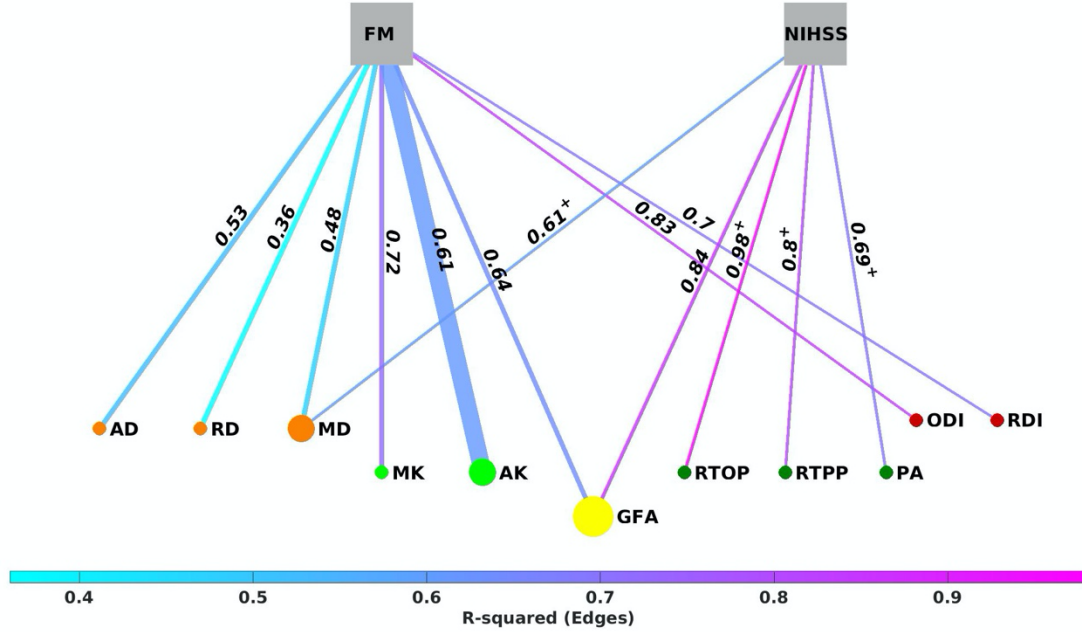


Figure 3: Summary of beyond DTI papers with outcomes (FM or NIHSS at ~1-3 months). The edge colors and labels are based on the 'best' R-squared value across papers for that pair. R-squared calculated from correlation where possible. A '+' sign indicates that other predictors (stroke size, age, etc) were a part of the joint model from which the R-squared is reported. We choose the 'best' vs. say, 'average' value across papers as some models maybe multivariate or report p-values (no correlations) making it harder to quantitatively combine across papers. Edge thickness (scaled across edges) is based on the total number of subjects from all the papers contributing to that edge. In our case, only two edges (between FM and AK and between FM and GFA) have multiple contributing papers. Node sizes/colors: Scaled based on number of papers from the pool using that particular diffusion parameter. We have removed redundancy in this calculation that arises from papers using the same data set.

While the papers with outcomes have significant heterogeneity making a traditional meta-analysis not possible, Figure 3 highlights that beyond DTI diffusion parameters report mostly better ability to predict or have significant correlations with motor outcome measurements compared to DTI parameters. The beyond DTI edge colors versus the DTI edge colors are roughly at two ends of the colorbar range.

Note that not all beyond DTI papers study outcome associations - so, the number of papers (node sizes) and number of subjects (edge thickness) in the graph underestimate the general enthusiasm and promising findings across the larger pool of papers covered in Tables 1 and 2.

The general rules followed to construct the graph (Fig. 3) were as follows:

- Within each paper, find reported correlation values between a given pair of diffusion parameter and a clinical score.
- If multiple papers use this pair, then choose the results which are unique.
For e.g., if the papers use the same data set, assign only one edge between the pair with the best R-Squared value for this edge across these papers (e.g., between NIHSS and GFA). However, if the papers are unique, then each paper's sample size adds to the edge thickness and the best R-Squared value across papers determines the edge color (e.g., between FM and GFA).
- Choosing 'best' r-squared value: In general, pick results with single-predictor models whenever possible. Multiple predictors in the model or multivariate analysis makes it harder to isolate the contribution of the exact diffusion parameter we are analyzing. The graph marks some edges with a '+' sign. These edges combine baseline measurements like stroke size, and age in the model and so the reported R-squared value of the edge is for the entire model and not the diffusion parameter alone.

Glossary

AD	Axial Diffusion. Computed from DTI - diffusion parallel to the primary eigenvector direction (the main fiber direction)
ADC	Apparent Diffusion Coefficient. The quantitative diffusion value in mm ² /s, termed “apparent” because of assumptions such as the distribution of diffusing spins is Gaussian. Note that when the diffusion value (ADC) is higher, the signal in diffusion-weighted images is lower.
AK	Axial Kurtosis. Non-Gaussian portion of diffusion signal in the direction parallel to the main fiber orientation
BCI	Brain Computer Interface. Could refer for example to a system with an EEG, processing, motor imagery, virtual reality, and functional electrical stimulation (FES)
Diffusion propagator	Also called 3D probability distribution function and ensemble average propagator (EAP). This fully characterizes the distribution of diffusion of water in a voxel, and can be used to derive other measures such as the ODF.
DKE	Diffusion Kurtosis Estimator. Open-source software for computing DKI parameters.
DKI	Diffusion Kurtosis Imaging. An extension to DTI to add a higher order term so that non-Gaussian non-linear processes can be modeled. Can generate mean kurtosis (MK), axial kurtosis (AK), radial kurtosis (RK), and other parameter sets such as WMTI

DTI	Diffusion Tensor Imaging. The acquisition of 6 or more diffusion weighted images and construction of a representative tensor at each location
DSI	Diffusion Spectrum Imaging. Acquisition with a large number of diffusion weightings (usually multiple b values and numerous directions) on a Cartesian grid to fill q-space
EAP	Ensemble Average Propagator. See diffusion propagator. (technically is an approximation of the average diffusion propagator, this depends on the narrow pulse condition)
fMRI	functional MRI. Method to detect blood flow changes with dynamic MRI, usually in the brain.
FA	Fractional Anisotropy, a measure of the directional diffusivity of water.
FM	Fugl-Meyer. Test of motor functions, FM upper extremity is 33 items each with values of 0,1,or 2. So the scale is 0-66. 66 is normal function. Named from Dr. Axel Fugl-Meyer, the first author of the survey.
FSL	FMRIB (Functional Magnetic Resonance Imaging of the Brain) Software Library. Widely used open-source tools for functional, structural, and diffusion MRI brain imaging datasets.
GFA	Generalized Fractional Anisotropy, measure of anisotropy from HARDI methods (std(ODF)/rms(ODF))

KA	Kurtosis Anisotropy. Also termed kurtosis fractional anisotropy (KFA) - similar to FA for the diffusion tensor, ranges 0-1 but is related to the directional variation of the non-Gaussian diffusion
mRS	Modified Rankin Scale. Ranges from 0-6. Standard scale for evaluating how well stroke patients can perform activities of daily living.
ND	Neurite Density. A parameter of the NODDI model that is related to how many neurites are in a voxel of region of interest. Note that in stroke areas, ND is not related to neurite density and is more of a restricted diffusion index (RDI)
NIHSS	National Institutes of Health stroke scale.
NODDI	Neurite Orientation Dispersion and Density Imaging. A model with intra-neurite (v_{ic} or ND or restricted diffusion index RDI), extra-neurite, and CSF (viso) compartments, and an ODI term.
ODF	Orientation Distribution Function. Representation of HARDI data. Can be created from the Funk-Radon Transform of single shell HARDI data, or by integrating 3D PDF from DSI
ODI	Orientation Dispersion Index. A parameter in the NODDI model that reflects how parallel nerve fibers are in a voxel, versus how dispersed in direction the fibers are.
q-space	Name given to diffusion-weighted space where the b value is the radius and the gradient weightings specify the direction. The 3D Fourier transform of q-space gives a 3D PDF, termed the diffusion propagator.

RD	Radial Diffusion. Computed from DTI - diffusion perpendicular to the primary eigenvector direction (the main fiber direction),
RDI	Restricted Diffusion Index. In the NODDI model, another term for neurite density ND or v_{ic} since in stroke the parameter may not reflect neurite density.
RTAP, RTPP	Return To the Axis Probability (RTAP) and the Return To the Plane Probability (RTPP) represent the integral of the EAP along the main diffusion direction and over the plane passing through the origin and perpendicular to the main diffusion direction, respectively.
SHORE	Simple Harmonic Oscillator Based Reconstruction and Estimation. A model based on Hermite functions for diffusion spectrum imaging data. Also extended to 3D SHORE and provides parameters RTAP, RTTP, and propagator anisotropy.
SMS	Simultaneous Multi-Slice. Also termed multi-band and hyperband. Method for exciting slices at the same time, typically with RF phase or slice gradient blips (CAIPIRINHA) to help separate the slices at reconstruction.
WMTI	White Matter Tract Integrity. A set of parameters that can be estimated from DKI data. The parameters include axonal diffusion (Da), extracellular diffusion (parallel and perpendicular De), tortuosity, and axonal water fraction (AWF).

References

1. Roger VL, Go AS, Lloyd-Jones DM, Adams RJ, Berry JD, Brown TM, . . . Wylie-Rosett J. Heart disease and stroke statistics--2011 update: a report from the American Heart Association. *Circulation* 2011;123:e18-e209
2. Kumar P, Kathuria P, Nair P, Prasad K. Prediction of Upper Limb Motor Recovery after Subacute Ischemic Stroke Using Diffusion Tensor Imaging: A Systematic Review and Meta-Analysis. *J Stroke* 2016;18:50-59
3. Puig J, Blasco G, Schlaug G, Stinear CM, Daunis IEP, Biarnes C, . . . Pedraza S. Diffusion tensor imaging as a prognostic biomarker for motor recovery and rehabilitation after stroke. *Neuroradiology* 2017;59:343-351
4. Moura LM, Luccas R, de Paiva JPQ, Amaro E, Jr., Leemans A, Leite CDC, . . . Conforto AB. Diffusion Tensor Imaging Biomarkers to Predict Motor Outcomes in Stroke: A Narrative Review. *Front Neurol* 2019;10:445
5. Hui ES, Fieremans E, Jensen JH, Tabesh A, Feng W, Bonilha L, . . . Helpern JA. Stroke Assessment With Diffusional Kurtosis Imaging. *Stroke; a journal of cerebral circulation* 2012
6. Granziera C, Daducci A, Meskaldji DE, Roche A, Maeder P, Michel P, . . . Krueger G. A new early and automated MRI-based predictor of motor improvement after stroke. *Neurology* 2012;79:39-46
7. Mastropietro A, Rizzo G, Fontana L, Figini M, Bernardini B, Straffi L, . . . Grimaldi M. Microstructural characterization of corticospinal tract in subacute and chronic stroke patients with distal lesions by means of advanced diffusion MRI. *Neuroradiology* 2019;61:1033-1045
8. Cramer SC, Nelles G, Benson RR, Kaplan JD, Parker RA, Kwong KK, . . . Rosen BR. A functional MRI study of subjects recovered from hemiparetic stroke. *Stroke* 1997;28:2518-2527
9. Hatem SM, Saussez G, Della Faille M, Prist V, Zhang X, Dispa D, Bleyenheuft Y. Rehabilitation of Motor Function after Stroke: A Multiple Systematic Review Focused on Techniques to Stimulate Upper Extremity Recovery. *Front Hum Neurosci* 2016;10:442
10. Liang D, Bhatta S, Gerzanich V, Simard JM. Cytotoxic edema: mechanisms of pathological cell swelling. *Neurosurg Focus* 2007;22:E2
11. Goyal M, Ospel JM, Menon B, Almekhlafi M, Jayaraman M, Fiehler J, . . . Fisher M. Challenging the Ischemic Core Concept in Acute Ischemic Stroke Imaging. *Stroke* 2020;51:3147-3155
12. Hori N, Carpenter DO. Functional and morphological changes induced by transient in vivo ischemia. *Exp Neurol* 1994;129:279-289
13. Baron CA, Kate M, Gioia L, Butcher K, Emery D, Budde M, Beaulieu C. Reduction of Diffusion-Weighted Imaging Contrast of Acute Ischemic Stroke at Short Diffusion Times. *Stroke* 2015;46:2136-2141
14. Zuo M, Guo H, Wan T, Zhao N, Cai H, Zha M, . . . Liu X. Wallerian degeneration in experimental focal cortical ischemia. *Brain Res Bull* 2019;149:194-202
15. Jones TA, Schallert T. Overgrowth and pruning of dendrites in adult rats recovering from neocortical damage. *Brain Res* 1992;581:156-160
16. Jones TA, Adkins DL. Motor System Reorganization After Stroke: Stimulating and Training Toward Perfection. *Physiology (Bethesda)* 2015;30:358-370
17. Alexander DC, Dyrby TB, Nilsson M, Zhang H. Imaging brain microstructure with diffusion MRI: practicality and applications. *NMR Biomed* 2019;32:e3841
18. Kiselev VG. Fundamentals of diffusion MRI physics. *NMR Biomed* 2017;30
19. Hagmann P, Jonasson L, Maeder P, Thiran JP, Wedeen VJ, Meuli R. Understanding diffusion MR imaging techniques: from scalar diffusion-weighted imaging to diffusion tensor imaging and beyond. *Radiographics* 2006;26 Suppl 1:S205-223

20. Novikov DS, Kiselev VG, Jespersen SN. On modeling. *Magn Reson Med* 2018;79:3172-3193
21. Tuch DS. Q-ball imaging. *Magn Reson Med* 2004;52:1358-1372
22. Concha L. A macroscopic view of microstructure: using diffusion-weighted images to infer damage, repair, and plasticity of white matter. *Neuroscience* 2014;276:14-28
23. Fukutomi H, Glasser MF, Zhang H, Autio JA, Coalson TS, Okada T, . . . Hayashi T. Neurite imaging reveals microstructural variations in human cerebral cortical gray matter. *Neuroimage* 2018;182:488-499
24. Palombo M, Ianus A, Guerreri M, Nunes D, Alexander DC, Shemesh N, Zhang H. SANDI: A compartment-based model for non-invasive apparent soma and neurite imaging by diffusion MRI. *Neuroimage* 2020;215:116835
25. Boscolo Galazzo I, Brusini L, Obertino S, Zucchelli M, Granziera C, Menegaz G. On the Viability of Diffusion MRI-Based Microstructural Biomarkers in Ischemic Stroke. *Front Neurosci* 2018;12:92
26. Schaefer PW, Grant PE, Gonzalez RG. Diffusion-weighted MR imaging of the brain. *Radiology* 2000;217:331-345
27. Duong TQ, Ackerman JJ, Ying HS, Neil JJ. Evaluation of extra- and intracellular apparent diffusion in normal and globally ischemic rat brain via ¹⁹F NMR. *Magn Reson Med* 1998;40:1-13
28. Jelescu IO, Veraart J, Fieremans E, Novikov DS. Degeneracy in model parameter estimation for multi-compartmental diffusion in neuronal tissue. *NMR Biomed* 2016;29:33-47
29. Dhital B, Reisert M, Kellner E, Kiselev VG. Intra-axonal diffusivity in brain white matter. *Neuroimage* 2019;189:543-550
30. Lampinen B, Szczepankiewicz F, Martensson J, van Westen D, Hansson O, Westin CF, Nilsson M. Towards unconstrained compartment modeling in white matter using diffusion-relaxation MRI with tensor-valued diffusion encoding. *Magn Reson Med* 2020;84:1605-1623
31. Budde MD, Frank JA. Neurite beading is sufficient to decrease the apparent diffusion coefficient after ischemic stroke. *Proceedings of the National Academy of Sciences of the United States of America* 2010;107:14472-14477
32. Datar A, Ameeramja J, Bhat A, Srivastava R, Mishra A, Bernal R, . . . Pullarkat PA. The Roles of Microtubules and Membrane Tension in Axonal Beading, Retraction, and Atrophy. *Biophys J* 2019;117:880-891
33. Brugieres P, Thomas P, Maraval A, Hosseini H, Combes C, Chafiq A, . . . Gaston A. Water diffusion compartmentation at high b values in ischemic human brain. *AJNR Am J Neuroradiol* 2004;25:692-698
34. Nilsson M, van Westen D, Stahlberg F, Sundgren PC, Latt J. The role of tissue microstructure and water exchange in biophysical modelling of diffusion in white matter. *Magma* 2013;26:345-370
35. Lampinen B, Latt J, Wasselius J, van Westen D, Nilsson M. Time dependence in diffusion MRI predicts tissue outcome in ischemic stroke patients. *Magn Reson Med* 2021;86:754-764
36. Kruetzelmann A, Kohrmann M, Sobesky J, Cheng B, Rosenkranz M, Rother J, . . . Thomalla G. Pretreatment diffusion-weighted imaging lesion volume predicts favorable outcome after intravenous thrombolysis with tissue-type plasminogen activator in acute ischemic stroke. *Stroke* 2011;42:1251-1254
37. Campbell BC, Tu HT, Christensen S, Desmond PM, Levi CR, Bladin CF, . . . Parsons MW. Assessing Response to Stroke Thrombolysis: Validation of 24-Hour Multimodal Magnetic Resonance Imaging. *Arch Neurol* 2011
38. Kim B, Winstein C. Can Neurological Biomarkers of Brain Impairment Be Used to Predict Poststroke Motor Recovery? A Systematic Review. *Neurorehabil Neural Repair* 2017;31:3-24

39. Kwah LK, Herbert RD. Prediction of Walking and Arm Recovery after Stroke: A Critical Review. *Brain Sci* 2016;6
40. Hemmen TM, Ernstrom K, Raman R. Two-hour improvement of patients in the national institute of neurological disorders and stroke trials and prediction of final outcome. *Stroke* 2011;42:3163-3167
41. Prabhakaran S, Zarahn E, Riley C, Speizer A, Chong JY, Lazar RM, . . . Krakauer JW. Inter-individual variability in the capacity for motor recovery after ischemic stroke. *Neurorehabil Neural Repair* 2008;22:64-71
42. Krakauer JW, Marshall RS. The proportional recovery rule for stroke revisited. *Ann Neurol* 2015;78:845-847
43. Winters C, van Wegen EE, Daffertshofer A, Kwakkel G. Generalizability of the Proportional Recovery Model for the Upper Extremity After an Ischemic Stroke. *Neurorehabil Neural Repair* 2015;29:614-622
44. Stinear CM, Byblow WD, Ackerley SJ, Smith MC, Borges VM, Barber PA. Proportional Motor Recovery After Stroke: Implications for Trial Design. *Stroke* 2017;48:795-798
45. Fugl-Meyer AR, Jaasko L, Leyman I, Olsson S, Steglind S. The post-stroke hemiplegic patient. 1. a method for evaluation of physical performance. *Scand J Rehabil Med* 1975;7:13-31
46. Hawe RL, Scott SH, Dukelow SP. Taking Proportional Out of Stroke Recovery. *Stroke* 2018;STROKEAHA118023006
47. Hope TMH, Friston K, Price CJ, Leff AP, Rotshtein P, Bowman H. Recovery after stroke: not so proportional after all? *Brain* 2019;142:15-22
48. Farr TD, Wegener S. Use of magnetic resonance imaging to predict outcome after stroke: a review of experimental and clinical evidence. *Journal of cerebral blood flow and metabolism : official journal of the International Society of Cerebral Blood Flow and Metabolism* 2010;30:703-717
49. Sun C, Liu X, Bao C, Wei F, Gong Y, Li Y, Liu J. Advanced non-invasive MRI of neuroplasticity in ischemic stroke: Techniques and applications. *Life Sci* 2020;261:118365
50. Albers GW, Thijs VN, Wechsler L, Kemp S, Schlaug G, Skalabrin E, . . . Marks MP. Magnetic resonance imaging profiles predict clinical response to early reperfusion: the diffusion and perfusion imaging evaluation for understanding stroke evolution (DEFUSE) study. *Ann Neurol* 2006;60:508-517
51. Qiu M, Darling WG, Morecraft RJ, Ni CC, Rajendra J, Butler AJ. White matter integrity is a stronger predictor of motor function than BOLD response in patients with stroke. *Neurorehabil Neural Repair* 2011;25:275-284
52. Carter AR, Shulman GL, Corbetta M. Why use a connectivity-based approach to study stroke and recovery of function? *NeuroImage* 2012;62:2271-2280
53. Zhu LL, Lindenberg R, Alexander MP, Schlaug G. Lesion load of the corticospinal tract predicts motor impairment in chronic stroke. *Stroke* 2010;41:910-915
54. Kumar MA, Vangala H, Tong DC, Campbell DM, Balgude A, Eyngorn I, . . . Albers GW. MRI guides diagnostic approach for ischaemic stroke. *J Neurol Neurosurg Psychiatry* 2011
55. Song J, Nair VA, Young BM, Walton LM, Nigogosyan Z, Remsik A, . . . Prabhakaran V. DTI measures track and predict motor function outcomes in stroke rehabilitation utilizing BCI technology. *Front Hum Neurosci* 2015;9:195
56. Puig J, Pedraza S, Blasco G, Daunis IEJ, Prats A, Prados F, . . . Serena J. Wallerian degeneration in the corticospinal tract evaluated by diffusion tensor imaging correlates with motor deficit 30 days after middle cerebral artery ischemic stroke. *AJNR Am J Neuroradiol* 2010;31:1324-1330
57. Groisser BN, Copen WA, Singhal AB, Hirai KK, Schaechter JD. Corticospinal tract diffusion abnormalities early after stroke predict motor outcome. *Neurorehabil Neural Repair* 2014;28:751-760

58. Jang SH, Lee J, Lee MY, Park SM, Choi WH, Do KH. Prediction of motor outcome using remaining corticospinal tract in patients with pontine infarct: Diffusion tensor imaging study. *Somatosens Mot Res* 2016;33:99-103
59. Pannek K, Chalk JB, Finnigan S, Rose SE. Dynamic corticospinal white matter connectivity changes during stroke recovery: a diffusion tensor probabilistic tractography study. *J Magn Reson Imaging* 2009;29:529-536
60. Kim KH, Kim YH, Kim MS, Park CH, Lee A, Chang WH. Prediction of Motor Recovery Using Diffusion Tensor Tractography in Supratentorial Stroke Patients With Severe Motor Involvement. *Ann Rehabil Med* 2015;39:570-576
61. Frank LR. Anisotropy in high angular resolution diffusion-weighted MRI. *Magn Reson Med* 2001;45:935-939
62. Tuch DS, Reese TG, Wiegell MR, Makris N, Belliveau JW, Wedeen VJ. High angular resolution diffusion imaging reveals intravoxel white matter fiber heterogeneity. *Magn Reson Med* 2002;48:577-582
63. Wedeen VJ, Wang RP, Schmahmann JD, Benner T, Tseng WY, Dai G, . . . de Crespigny AJ. Diffusion spectrum magnetic resonance imaging (DSI) tractography of crossing fibers. *Neuroimage* 2008;41:1267-1277
64. Van AT, Granziera C, Bammer R. An introduction to model-independent diffusion magnetic resonance imaging. *Top Magn Reson Imaging* 2010;21:339-354
65. Jones DK, Knosche TR, Turner R. White matter integrity, fiber count, and other fallacies: The do's and don'ts of diffusion MRI. *NeuroImage* 2012
66. Lakhani DA, Schilling KG, Xu J, Bagnato F. Advanced Multicompartment Diffusion MRI Models and Their Application in Multiple Sclerosis. *AJNR Am J Neuroradiol* 2020;41:751-757
67. Jensen JH, Helpern JA, Ramani A, Lu H, Kaczynski K. Diffusional kurtosis imaging: the quantification of non-gaussian water diffusion by means of magnetic resonance imaging. *Magn Reson Med* 2005;53:1432-1440
68. Lu H, Jensen JH, Ramani A, Helpern JA. Three-dimensional characterization of non-gaussian water diffusion in humans using diffusion kurtosis imaging. *NMR Biomed* 2006;19:236-247
69. Cheung JS, Wang E, Lo EH, Sun PZ. Stratification of heterogeneous diffusion MRI ischemic lesion with kurtosis imaging: evaluation of mean diffusion and kurtosis MRI mismatch in an animal model of transient focal ischemia. *Stroke* 2012;43:2252-2254
70. Hui ES, Du F, Huang S, Shen Q, Duong TQ. Spatiotemporal dynamics of diffusional kurtosis, mean diffusivity and perfusion changes in experimental stroke. *Brain research* 2012;1451:100-109
71. Sun PZ, Wang Y, Mandeville E, Chan ST, Lo EH, Ji X. Validation of fast diffusion kurtosis MRI for imaging acute ischemia in a rodent model of stroke. *NMR Biomed* 2014;27:1413-1418
72. Umesh Rudrapatna S, Wieloch T, Beirup K, Ruscher K, Mol W, Yanev P, . . . Dijkhuizen RM. Can diffusion kurtosis imaging improve the sensitivity and specificity of detecting microstructural alterations in brain tissue chronically after experimental stroke? Comparisons with diffusion tensor imaging and histology. *Neuroimage* 2014;97:363-373
73. Weber RA, Hui ES, Jensen JH, Nie X, Falangola MF, Helpern JA, Adkins DL. Diffusional kurtosis and diffusion tensor imaging reveal different time-sensitive stroke-induced microstructural changes. *Stroke* 2015;46:545-550
74. Wu Y, Kim J, Chan ST, Zhou IY, Guo Y, Igarashi T, . . . Sun PZ. Comparison of image sensitivity between conventional tensor-based and fast diffusion kurtosis imaging protocols in a rodent model of acute ischemic stroke. *NMR Biomed* 2016;29:625-630
75. Zhang S, Yao Y, Shi J, Tang X, Zhao L, Zhu W. The temporal evolution of diffusional kurtosis imaging in an experimental middle cerebral artery occlusion (MCAO) model. *Magn Reson Imaging* 2016;34:889-895

76. Wang E, Wu Y, Cheung JS, Zhou IY, Igarashi T, Zhang X, Sun PZ. pH imaging reveals worsened tissue acidification in diffusion kurtosis lesion than the kurtosis/diffusion lesion mismatch in an animal model of acute stroke. *J Cereb Blood Flow Metab* 2017;37:3325-3333
77. Lu D, Jiang Y, Ji Y, Zhou IY, Mandeville E, Lo EH, . . . Sun PZ. JOURNAL CLUB: Evaluation of Diffusion Kurtosis Imaging of Stroke Lesion With Hemodynamic and Metabolic MRI in a Rodent Model of Acute Stroke. *AJR Am J Roentgenol* 2018;210:720-727
78. Bay V, Kjolby BF, Iversen NK, Mikkelsen IK, Ardalan M, Nyengaard JR, . . . Hansen B. Stroke infarct volume estimation in fixed tissue: Comparison of diffusion kurtosis imaging to diffusion weighted imaging and histology in a rodent MCAO model. *PLoS One* 2018;13:e0196161
79. Cheung J, Doerr M, Hu R, Sun PZ. Refined Ischemic Penumbra Imaging with Tissue pH and Diffusion Kurtosis Magnetic Resonance Imaging. *Transl Stroke Res* 2021;12:742-753
80. Puig J, Pedraza S, Blasco G, Daunis IEJ, Prados F, Remollo S, . . . Serena J. Acute damage to the posterior limb of the internal capsule on diffusion tensor tractography as an early imaging predictor of motor outcome after stroke. *AJNR Am J Neuroradiol* 2011;32:857-863
81. Hansen B, Jespersen SN. Recent Developments in Fast Kurtosis Imaging. *Frontiers in Physics* 2017;5
82. Spampinato MV, Chan C, Jensen JH, Helpern JA, Bonilha L, Kautz SA, . . . Feng W. Diffusional Kurtosis Imaging and Motor Outcome in Acute Ischemic Stroke. *AJNR Am J Neuroradiol* 2017;38:1328-1334
83. Li C, Lan C, Zhang X, Yin L, Hao X, Tian J, . . . Yang Y. Evaluation of Diffusional Kurtosis Imaging in Sub-acute Ischemic Stroke: Comparison with Rehabilitation Treatment Effect. *Cell Transplant* 2019;28:1053-1061
84. Yu X, Jiaerken Y, Wang S, Hong H, Jackson A, Yuan L, . . . Huang P. Changes in the Corticospinal Tract Beyond the Ischemic Lesion Following Acute Hemispheric Stroke: A Diffusion Kurtosis Imaging Study. *J Magn Reson Imaging* 2020;52:512-519
85. Chung S, Fieremans E, Wang X, Kucukboyaci NE, Morton CJ, Babb J, . . . Lui YW. White Matter Tract Integrity: An Indicator of Axonal Pathology after Mild Traumatic Brain Injury. *J Neurotrauma* 2018;35:1015-1020
86. Wedeen VJ, Hagmann P, Tseng WY, Reese TG, Weisskoff RM. Mapping complex tissue architecture with diffusion spectrum magnetic resonance imaging. *Magn Reson Med* 2005;54:1377-1386
87. Jiang Q, Zhang ZG, Chopp M. MRI evaluation of white matter recovery after brain injury. *Stroke* 2010;41:S112-113
88. Tang PF, Ko YH, Luo ZA, Yeh FC, Chen SH, Tseng WY. Tract-specific and region of interest analysis of corticospinal tract integrity in subcortical ischemic stroke: reliability and correlation with motor function of affected lower extremity. *AJNR Am J Neuroradiol* 2010;31:1023-1030
89. Granziera C, Daducci A, Gigandet X, Cammoun L, Djalel ME, Michel P, . . . Krueger G. Diffusion spectrum imaging after stroke shows structural changes in the contra-lateral motor network correlating with functional recovery. *Int Soc Magn Reson Med.* Montreal; 2011:4199
90. Ozarslan E, Koay CG, Shepherd TM, Komlosh ME, Irfanoglu MO, Pierpaoli C, Bassar PJ. Mean apparent propagator (MAP) MRI: a novel diffusion imaging method for mapping tissue microstructure. *Neuroimage* 2013;78:16-32
91. Brusini L, Obertino S, Galazzo IB, Zucchelli M, Krueger G, Granziera C, Menegaz G. Ensemble average propagator-based detection of microstructural alterations after stroke. *Int J Comput Assist Radiol Surg* 2016;11:1585-1597
92. Zhang H, Schneider T, Wheeler-Kingshott CA, Alexander DC. NODDI: practical in vivo neurite orientation dispersion and density imaging of the human brain. *Neuroimage* 2012;61:1000-1016

93. Anderova M, Vorisek I, Pivonkova H, Benesova J, Vargova L, Cicanic M, . . . Sykova E. Cell death/proliferation and alterations in glial morphology contribute to changes in diffusivity in the rat hippocampus after hypoxia-ischemia. *J Cereb Blood Flow Metab* 2011;31:894-907
94. Bagdasarian FA, Yuan X, Athey J, Bunnell BA, Grant SC. NODDI highlights recovery mechanisms in white and gray matter in ischemic stroke following human stem cell treatment. *Magn Reson Med* 2021
95. Adluru G, Gur Y, Anderson J, Richards LG, Adluru N, DiBella EVR. Assessment of white matter microstructure in stroke patients using NODDI. *IEEE Eng in Med and Biol (EMBC)*. Chicago, IL; 2014:PMC4325943
96. Hodgson K, Adluru G, Richards LG, Majersik JJ, Stoddard G, Adluru N, DiBella E. Predicting motor outcomes in stroke patients using diffusion spectrum MRI microstructural measures. *Frontiers in Neurology, section Applied Neuroimaging* 2019;10:72
97. Wang Z, Zhang S, Liu C, Yao Y, Shi J, Zhang J, . . . Zhu W. A study of neurite orientation dispersion and density imaging in ischemic stroke. *Magn Reson Imaging* 2019;57:28-33
98. Latt J, Nilsson M, van Westen D, Wirestam R, Stahlberg F, Brockstedt S. Diffusion-weighted MRI measurements on stroke patients reveal water-exchange mechanisms in sub-acute ischaemic lesions. *NMR Biomed* 2009;22:619-628
99. Barrio-Arranz G, de Luis-Garcia R, Tristan-Vega A, Martin-Fernandez M, Aja-Fernandez S. Impact of MR Acquisition Parameters on DTI Scalar Indexes: A Tractography Based Approach. *PLoS One* 2015;10:e0137905
100. Parvathaneni P, Nath V, Blaber JA, Schilling KG, Hainline AE, Mojahed E, . . . Landman BA. Empirical reproducibility, sensitivity, and optimization of acquisition protocol, for Neurite Orientation Dispersion and Density Imaging using AMICO. *Magn Reson Imaging* 2018;50:96-109
101. Bergamino M, Keeling EG, Walsh RR, Stokes AM. Systematic Assessment of the Impact of DTI Methodology on Fractional Anisotropy Measures in Alzheimer's Disease. *Tomography* 2021;7:20-38
102. Daducci A, Canales-Rodriguez EJ, Zhang H, Dyrby TB, Alexander DC, Thiran JP. Accelerated Microstructure Imaging via Convex Optimization (AMICO) from diffusion MRI data. *Neuroimage* 2015;105:32-44
103. HashemizadehKolowri K, Chen R-R, Adluru G, Dean DC, Wilde EA, Alexander AL, DiBella E. Simultaneous multi-slice image reconstruction using regularized image domain split slice-GRAPPA for diffusion MRI. *Med Image Anal* 2021;70:102000
104. Ye C, Li Y, Zeng X. An improved deep network for tissue microstructure estimation with uncertainty quantification. *Med Image Anal* 2020;61:101650
105. Bundy DT, Souders L, Baranyai K, Leonard L, Schalk G, Coker R, . . . Leuthardt EC. Contralesional Brain-Computer Interface Control of a Powered Exoskeleton for Motor Recovery in Chronic Stroke Survivors. *Stroke* 2017;48:1908-1915
106. Jensen JH, Falangola MF, Hu C, Tabesh A, Rapalino O, Lo C, Helpern JA. Preliminary observations of increased diffusional kurtosis in human brain following recent cerebral infarction. *NMR in biomedicine* 2011;24:452-457
107. Zhang S, Zhu W, Zhang Y, Yao Y, Shi J, Wang CY, Zhu W. Diffusional kurtosis imaging in evaluating the secondary change of corticospinal tract after unilateral cerebral infarction. *Am J Transl Res* 2017;9:1426-1434
108. Chou MC, Ko CW, Chiu YH, Chung HW, Lai PH. Effects of B Value on Quantification of Rapid Diffusion Kurtosis Imaging in Normal and Acute Ischemic Brain Tissues. *J Comput Assist Tomogr* 2017;41:868-876
109. Chen H, Jiang L, Zhang H, Zhang YD, Geng W, Feng Y, . . . Yin X. Corticospinal tract changes in acute brainstem ischemic stroke patients: A diffusion kurtosis imaging study. *Neurology India* 2018;66:726-732

110. Yin J, Sun H, Wang Z, Ni H, Shen W, Sun PZ. Diffusion Kurtosis Imaging of Acute Infarction: Comparison with Routine Diffusion and Follow-up MR Imaging. *Radiology* 2018;287:651-657
111. Zhu LH, Zhang ZP, Wang FN, Cheng QH, Guo G. Diffusion kurtosis imaging of microstructural changes in brain tissue affected by acute ischemic stroke in different locations. *Neural Regen Res* 2019;14:272-279
112. Lin YC, Daducci A, Meskaldji DE, Thiran JP, Michel P, Meuli R, . . . Granziera C. Quantitative Analysis of Myelin and Axonal Remodeling in the Uninjured Motor Network After Stroke. *Brain Connect* 2015;5:401-412